

INTEGRATED OPTICS

PACS numbers: 42.82.Bq; 42.79.Sz; 07.60.Ly
DOI: 10.1070/QE2009v039n03ABEH013972

Properties of an ultrafast all-optical switching window in an integrated silicon-based Mach – Zehnder interferometer

Jianwei Wu, Fengguang Luo, Zhihua Yu, Qing Tao

Abstract. **An ultrafast all-optical switch based on the integrated Mach – Zehnder interferometer (MZI) with two arms consisting of identical silicon-on-insulator (SOI) optical waveguides is presented. The operability of the presented interferometer is simulated both for the continue wave (cw) and pulsed probe signals. It is shown that at the output port of the MZI, the switching window of the probe signal is strongly dependent on the energy and duration of the ultrafast control pulse and the SOI waveguide length. In addition, the initial delay time between both two optical waves will significantly affect the optical switching window when a pulsed probe signal wave is used.**

Keywords: *integrated optics, silicon-on-insulator technology, Mach – Zehnder interferometer, ultrafast all-optical switching.*

1. Introduction

Ultrafast all-optical switching has attracted much interest due to its potential applications in the field of optical communications such as optical time division multiplexing (OTDM) and 3R systems, etc. So far, various kinds of all-optical switching devices have been proposed and demonstrated, in which the optical switching with the well-known Mach – Zehnder interferometer (MZI) configuration seems to be the most popular because of its simple design and fabrication. Different waveguide switches based on MZI configurations have been previously studied and implemented to realise the switching function. However, the development of integrated optoelectronics necessitates an urgent demand for integrated MZI structures. We have developed a silicon-based MZI because in recent years, silicon photonics has been attracting more and more attention due to its potential for integrated optics [1, 2].

Many new types of nonlinear optical phenomena such as two-photon absorption (TPA), TPA-induced free carrier absorption, and free carrier dispersion (FCD), etc. have been successfully demonstrated and thoroughly investigated in silicon-based nanophotonic devices, where the SOI waveguides are especially promising for application due to the SOI structure. An optical SOI waveguide has a silicon core with the refractive index $n \simeq 3.5$ surrounded by a SiO_2 cladding with $n \simeq 1.5$, which provides a high index contrast between the silicon core and cladding, and, therefore, the optical field is confined in the silicon layer with a small cross section. As a consequence, nonlinear processes including the Kerr effect, etc., are more intense in a SOI waveguide compared to those in conventional well-studied fibre waveguides, which are widely used to design different functional elements.

Based on the aforesaid, in this paper we present and analyse the silicon-based MZI configuration proposed in [3]. However, Zhou et al. [3] demonstrated only the filtering properties of the MZI. Thus, other applications based on the MZI need still be further explored and investigated. Taking this into account, the capabilities of the SOI-based MZI configuration were extended, which allowed us to implement the ultrafast all-optical switching. The properties of the optical switching windows are thoroughly investigated for cw and pulsed probe signal waves by varying the energy and duration of the control pulse, the waveguide length, and the initial delay time.

2. Device and principles of the waveguide switch operation

Figure 1 presents the developed MZI configuration and the ridge SOI waveguide cross section. Two identical SOI waveguides (Fig. 1a) are placed respectively at the upper arm (phase-modulating arm) and lower arm (reference arm) of the MZI. In Fig. 1, Y1 and Y2 are the 3-dB Y-couplers, C1 and C2 are the 3-dB directional couplers, and F is the filter which cuts off the control pulse. The operation principle of the optical switch can be described as follows: the probe signal is equally distributed between the upper and lower arms of the MZI by the C1-coupler, and then, before entering the SOI waveguide, a part of the probe signal will be combined with the control pulse in the upper arm. In the SOI waveguide, the probe signal experiences an additional phase shift due to the nonlinear action of the control pulse. In the reference arm, only a part of the probe signal directly passes through the SOI waveguide. As a result, the phase difference between both parts of the divided probe signals after propagating through the SOI waveguide provides ultrafast all-optical switching at the

Jianwei Wu College of Mathematics and Physics, Hohai University, Nanjing 210098, P.R. China;
Fengguang Luo, Zhihua Yu, Qing Tao Wuhan National Laboratory for Optoelectronics, Wuhan 430074, P.R. China; College of Optoelectronics Science and Engineering, Huazhong University of Science and Technology, Wuhan 430074, P.R. China; e-mail: jwwu@hhu.edu.cn

Received 24 August 2008
Kvantovaya Elektronika **39** (3) 293 – 297 (2009)
Submitted in English

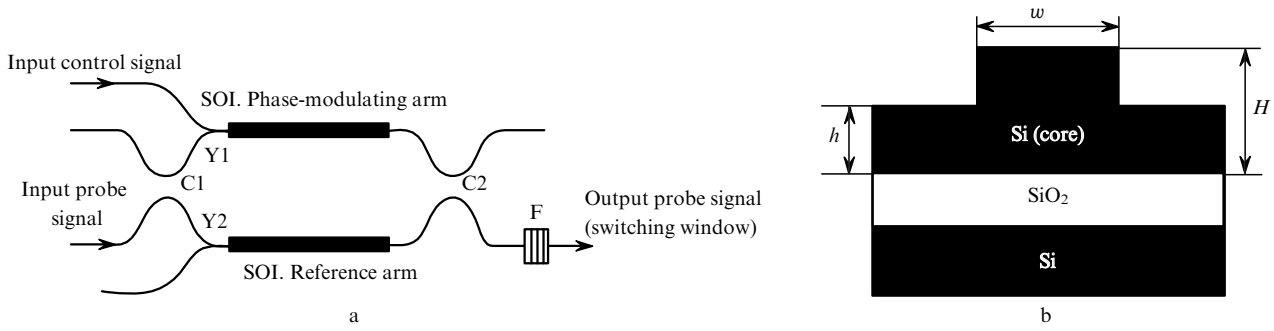

Figure 1. Scheme of the MZI (a) and the cross section of a ridge SOI waveguide (b).

down output port of the MZI. If the control pulse is not fed at the input port, the energy of output probe signal is zero at the down output port, i.e. the probe signal is completely turned off because of the phase difference π induced by the two 3-dB directional couplers.

Figure 1b shows the structure of a ridge SOI waveguide of width w, rib height H, and slab height h. Upon propagation of optical waves, free carriers will accumulate in the SOI waveguide. The effective recombination lifetime τ_{eff}^{-1} of these carriers may be denoted by [4]

$$\tau_{\text{eff}}^{-1} = \frac{S}{H} + \frac{w + 2(H-h)}{wH} S' + 2\frac{h}{H}\left[\frac{D}{w^2}\left(\frac{S+S'}{h}\right)\right]^{1/2}, \quad (1)$$

where the first term determines the recombination lifetime at the interface, the second term corresponds to the surface recombination at the sidewalls, and the last term refers to the transit time out of the interaction region; S and S' are the effective surface recombination velocities; D is the diffusion coefficient.

The nonlinear transfer equations modified for the control and probe waves in the phase-modulating arm of the SOI waveguide have the form [5, 6]

$$\frac{\partial A_{\text{c}}}{\partial z} + \beta_{\text{c1}}\frac{\partial A_{\text{c}}}{\partial t} + \text{i}\frac{1}{2}\beta_{\text{c2}}\frac{\partial^2 A_{\text{c}}}{\partial t^2} - \frac{1}{6}\beta_{\text{c3}}\frac{\partial^3 A_{\text{c}}}{\partial t^3}$$

$$= -\frac{1}{2}\alpha_{\text{c1}}A_{\text{c}} - \frac{1}{2}\alpha_{\text{cFC}}A_{\text{c}} - \frac{1}{2}\frac{\beta_{\text{ccTPA}}}{B_{\text{c eff}}}|A_{\text{c}}|^2 A_{\text{c}} - \frac{\beta_{\text{cdTPA}}}{B_{\text{c eff}}}|A_{\text{d}}|^2 A_{\text{c}}$$

$$+ \text{i}\gamma_{\text{c,c}}|A_{\text{c}}|^2 A_{\text{c}} + \text{i}2\gamma_{\text{c,d}}|A_{\text{d}}|^2 A_{\text{c}} + \text{i}\frac{2\pi}{\lambda_{\text{c}}}\Delta n_{\lambda\text{c}} A_{\text{c}}, \quad (2)$$

$$\frac{\partial A_{\text{d}}}{\partial z} + \beta_{\text{d1}}\frac{\partial A_{\text{d}}}{\partial t} + \text{i}\frac{1}{2}\beta_{\text{d2}}\frac{\partial^2 A_{\text{d}}}{\partial t^2} - \frac{1}{6}\beta_{\text{d3}}\frac{\partial^3 A_{\text{d}}}{\partial t^3}$$

$$= -\frac{1}{2}\alpha_{\text{d1}}A_{\text{d}} - \frac{1}{2}\alpha_{\text{dFC}}A_{\text{d}} - \frac{1}{2}\frac{\beta_{\text{ddTPA}}}{B_{\text{d eff}}}|A_{\text{d}}|^2 A_{\text{d}} - \frac{\beta_{\text{dcTPA}}}{B_{\text{d eff}}}|A_{\text{c}}|^2 A_{\text{d}}$$

$$+ \text{i}\gamma_{\text{d,d}}|A_{\text{d}}|^2 A_{\text{d}} + \text{i}2\gamma_{\text{d,c}}|A_{\text{c}}|^2 A_{\text{d}} + \text{i}\frac{2\pi}{\lambda_{\text{d}}}\Delta n_{\lambda\text{d}} A_{\text{d}}. \quad (3)$$

The transfer equation of the probe wave in the reference arm of the SOI waveguide has the form

$$\frac{\partial A_{\text{d}}}{\partial z} + \beta_{\text{d1}}\frac{\partial A_{\text{d}}}{\partial t} = -\frac{1}{2}\alpha_{\text{d1}}A_{\text{d}} - \frac{1}{2}\alpha_{\text{dFC}}A_{\text{d}} - \frac{1}{2}\frac{\beta_{\text{ddTPA}}}{B_{\text{d eff}}}|A_{\text{d}}|^2 A_{\text{d}}$$

$$+ \text{i}\gamma_{\text{d,d}}|A_{\text{d}}|^2 A_{\text{d}} + \text{i}\frac{2\pi}{\lambda_{\text{d}}}\Delta n_{\lambda\text{d}} A_{\text{d}}, \quad (4)$$

where subscripts c and d denote the control pulse and probe signal, respectively; A is a slowly varying pulse envelope; β_1, β_2, and β_3 are the first-, second-, and third-order dispersion coefficients. The parameter β_1 is inversely proportional to the group velocity of the pulse as $v_{\text{g}} = 1/\beta_1$, while β_2 governs the effect of the group-velocity dispersion (GVD), and β_3 is responsible for the effects of the third-order dispersion (TOD) and becomes important for ultrashort pulses because of their wide bandwidth. The quantity $\gamma = 2\pi n_2/\lambda B_{\text{eff}}$ is a nonlinear parameter; n_2 is a nonlinear coefficient; B_{eff} is the effective core area; λ is the central wavelength of the optical wave; α_1 is the linear propagation loss; α_{FC} is the free-carrier absorption (FCA) coefficient; β_{TPA} is the two-photon absorption coefficient, which has identical values for all kinds of TPA processes; and ω is the angle frequency. The first four terms in the right-hand side of Eqns (2) and (3) denote the propagation loss, FCA loss, degenerate TPA and non-degenerate TPA, respectively. The next two terms represent the self-phase modulation (SPM) and cross-phase modulation (XPM), respectively, and the final term describes the free carrier dispersion related to the efficient index change Δn which can be written in the form

$$\Delta n_{\lambda\text{c,d}} = -8.8\times10^{-22}\left(\frac{\lambda_{\text{cd}}}{1.55}\right)^2\Delta n_{\text{e}} - 8.5\times10^{-18}\left(\frac{\lambda_{\text{cd}}}{1.55}\right)^2(\Delta n_{\text{h}})^{0.8}; \quad (5)$$

and the FCA coefficient is written in the form

$$\alpha_{\text{FC}} = 8.5\times10^{-18}\left(\frac{\lambda_{\text{cd}}}{1.55}\right)^2\Delta n_{\text{e}} + 6.0\times10^{-18}\left(\frac{\lambda_{\text{cd}}}{1.55}\right)^2\Delta n_{\text{h}} = \sigma n_{\text{eh}} = \sigma_0\left(\frac{\lambda_{\text{cd}}}{1.55}\right)^2 n_{\text{eh}}, \quad (6)$$

where $\sigma_0 = 1.45\times10^{-7}$ cm^2 is the free-carrier absorption cross section measured at 1.55 μm [7]; $n_{\text{eh}} = n_{\text{e}} = n_{\text{h}}$ is the density of electron–hole pairs generated by the degenerate TPA and non-degenerated TPA processes, which is given by the equation

$$\frac{\text{d}n_{\text{eh}}}{\text{d}T} = -\frac{n_{\text{eh}}}{\tau_{\text{eff}}} + \frac{\beta_{\text{ccTPA}}}{2\eta\omega_{\text{c}}}\left(|A_{\text{c}}(z,t)|^2 B_{\text{c eff}}^{-1}\right)^2 + \frac{\beta_{\text{ddTPA}}}{2\eta\omega_{\text{d}}}\left(|A_{\text{d}}(z,t)|^2 B_{\text{d eff}}^{-1}\right)^2 + \frac{\beta_{\text{cdTPA}}}{\eta\omega_{\text{d}}}\left(|A_{\text{d}}(z,t)|^2|A_{\text{c}}(z,t)|^2 B_{\text{c eff}}^{-1}\right)^2 +$$

$$+\frac{\beta_{\mathrm{dcTPA}}}{\eta\omega_{\mathrm{c}}}\left(|A_{\mathrm{c}}(z,t)|^2|A_{\mathrm{d}}(z,t)|^2B_{\mathrm{d\,eff}}^{-1}\right)^2. \quad (7)$$

To observe the properties of the obtained ultrafast all-optical switching window, Eqns (1)–(7) with determined boundary conditions can be solved numerically. In the following sections, the detailed results of simulations are presented.

3. Numerical simulations and discussion of the results

Parameters used in simulations correspond to data borrowed from [4, 8] and are presented below.

Control pulse wavelength $\lambda_{\mathrm{c}}/\mathrm{nm}$	1550
Probe signal wavelength $\lambda_{\mathrm{d}}/\mathrm{nm}$	1650
Nonlinear coefficient $n_2/\mathrm{m^2\ W^{-1}}$	6×10^{-18}
First-order dispersion coefficient at the pump wavelength $\beta_{\mathrm{c1}}/\mathrm{s\ m^{-1}}$	7.3960×10^{-8}
Second-order dispersion coefficient at the pump wavelength β_{c2}	0
Third-order dispersion coefficient at the pump wavelength $\beta_{\mathrm{c3}}/\mathrm{ps^3\ m^{-1}}$	4.0×10^{-3}
First-order dispersion coefficient at the cw wavelength $\beta_{\mathrm{d1}}/\mathrm{s\ m^{-1}}$	7.3836×10^{-8}
Second-order dispersion coefficient at the cw wavelength $\beta_{\mathrm{d2}}/\mathrm{ps^2\ m^{-1}}$	−0.3
Third-order dispersion coefficient at the cw wavelength $\beta_{\mathrm{d3}}/\mathrm{ps^3\ m^{-1}}$	4.1×10^{-3}
Waveguide linear loss coefficient $\alpha_{\mathrm{cl,dl}}/\mathrm{dB\ cm^{-1}}$	0.22
Two-photon absorption coefficient $\beta_{\mathrm{TPA}}/\mathrm{cm\ GW^{-1}}$	0.5
Rib waveguide width w/nm	900
Rib height H/nm	780
Slab height h/nm	390
Effective surface recombination velocity $S, S'/\mathrm{m\ s^{-1}}$	80
Diffusion coefficient $D/\mathrm{cm^2\ s^{-1}}$	16
Reduced Planck's constant $\hbar/\mathrm{J\ s}$	1.06×10^{-34}

We performed numerical simulations to study the properties of switching windows based on the silicon-based MZI configuration. Figure 2 shows the output switching window and the corresponding phase differences between the phase-modulating and reference arms at the input powers of the control pulse, $P_{\mathrm{c0}}=1$, 2 and 5W, respectively. In the simulation, the SOI waveguide length was $L=15$ mm, the initial duration of the control pulse at the 1/e intensity level was $T_{\mathrm{c0}}=100$ fs, the input power of the cw probe signal was $P_{\mathrm{d0}}=100$ mW, and the control pulse had a Gaussian profile. Some important conclusions can be drawn from Fig. 2a: when the initial peak power of the control pulse is increased from 1 to 5 W, the energy of the outcoming switching window will be enhanced quickly, and the switching window will be also remarkably distorted, i.e. a high-power and long peak appears at the trailing edge, and the pulse itself is shifted in time with respect to the control pulse. This phenomenon can be explained as follows: when the control pulse is introduced into the SOI waveguide, it will act on the copropagating probe signal wave in a nonlinear way, including XPM, TPA, FCA, and FCD, etc. As a result, the phase of the probe signal wave changes, namely, the phase difference between the interferometer arms is not equal to π, which is induced by the two directional couplers (Fig. 2b). As a consequence, the switching window is turned on. When the power of the input control pulse is small ($P_{\mathrm{c0}}=1$ W), such nonlinear processes as FCA and FCD can be neglected because the accumulation of free carriers mainly induced by the control pulse is very small at a low power level. As a result, the additional phase shift of the probe signal wave is induced mainly by the XPM and TPA in the phase-modulating arm, which results in a nearly symmetric switching window. However, when the input power of the control pulse is increased to 2 W and higher, we should take into account the free carrier effect leading to a larger phase shift between the phase-modulating and reference arms after passing through the interferometer. Because of this, the switching window achieves has a high energy level. Because the refractive index of the waveguide changes significantly with increasing the free carrier density, the phase difference between the probe signal and the lagging control pulse will also change. In this case, the switching window takes on a long tail whose power will increase with increasing the control pulse power. Note that the switching window is shifted backward in time with respect to the control pulse because the group velocity of the probe signal wave is slower than that of the control pulse.

Figure 3 shows the changes in the amplitude of the switching window and the corresponding phase shifts at $P_{\mathrm{c0}}=1$ W, $L=15$ mm, $P_{\mathrm{d0}}=100$ mW and different durations of the control pulse. When T_{c0} is increased, the switching window is quickly broadened. This can be explained by the fact that the overlapped region is increased due to the increased pulse duration. As a result, the range of the phase change for the probe signal is also increased (Fig. 3b), which leads to broadening of the output switching window. However, the free carrier density will increase with increasing the duration of the control pulse so that the tail

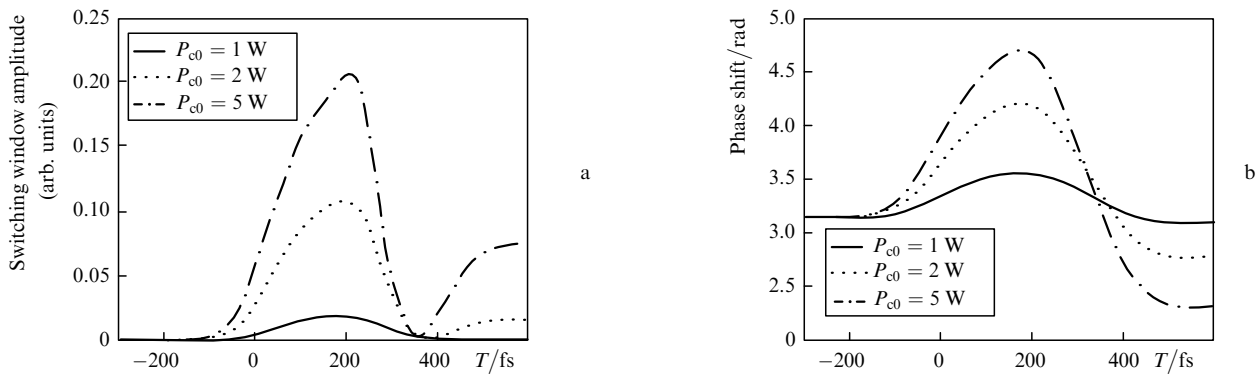

Figure 2. Amplitudes of the output switching window (a) and the corresponding phase shifts (b) at different powers of the input control signal.

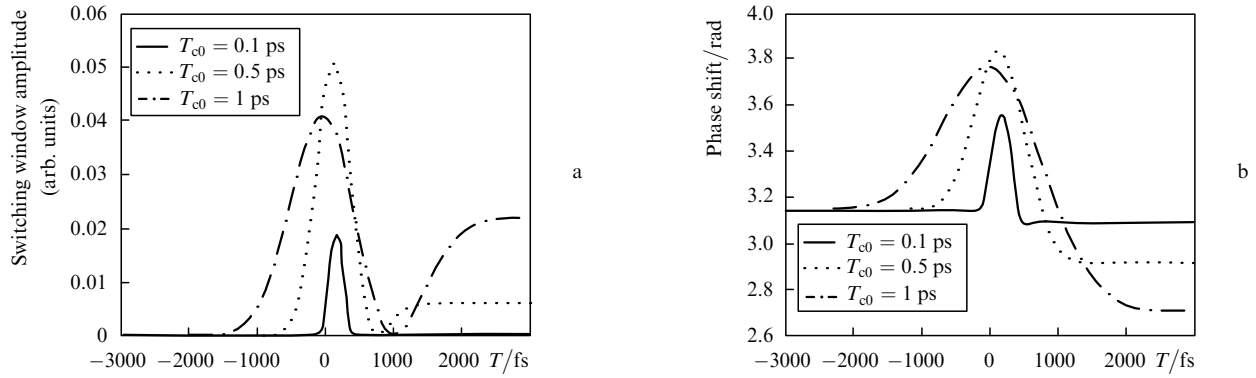

Figure 3. Amplitudes of the output switching window (a) and the corresponding phase shifts (b) at different durations of the input control signal.

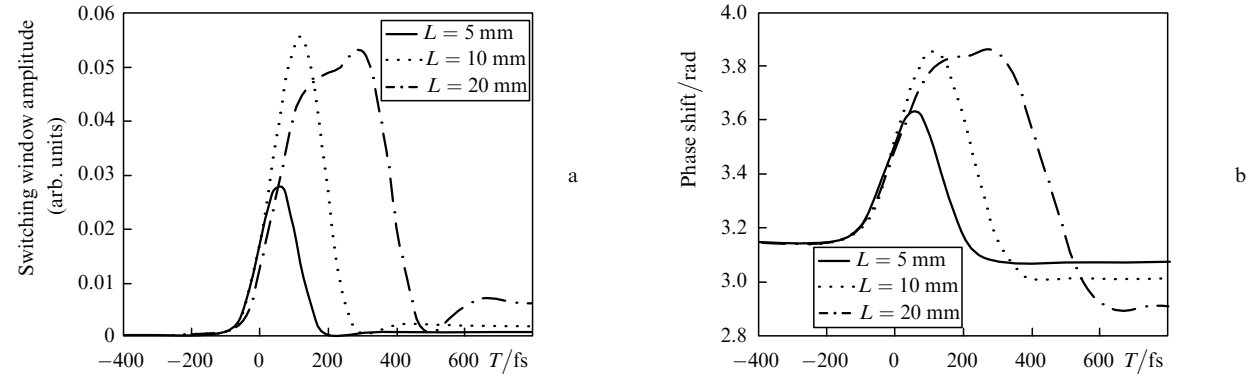

Figure 4. Amplitudes of the output switching window (a) and the corresponding phase shifts (b) at different lengths of the waveguide.

of the extended switching window is enhanced remarkably at $T_{c0} = 0.5$ and 1 ps. This phenomenon can be explained in a similar way to the above analysis of Fig. 2.

In fact, the waveguide length will similarly influence the properties of the switching window (Fig. 4a). The simulation parameters are: $T_{c0} = 100$ fs, $P_{c0} = 2$ W and $P_{d0} = 100$ mW. It is obvious that the switching window is broadened by increasing the waveguide length because of the group-velocity mismatch between the control and probe wave. Note that the output energy increases with increasing the waveguide length from 5 to 10 mm, which can be explained by the fact that the nonlinear interaction length increases with stretching the waveguide length. As a result, the corresponding phase shift shown in Fig. 4b is also increased. At the same time, at $L = 20$ mm the peak power of the switching window falls down compared to the case when $L = 10$ mm because the nonlinear losses increase with the waveguide length.

We simulated numerically the pulsed probe signal wave for its comparison with the cw probe signal. In calculations, a 100-fs Gaussian probe pulse is considered at the 1/e intensity level. Figure 5 shows the amplitudes of the output switching window upon varying the power and duration of the control pulse, and the waveguide length. One can see that when the corresponding parameters are changed, the evolution of the switching window is similar to the case of the cw probe signal. The physical explanation of the evolution is also identical to the above analysis of Figs 2–4. For example, when the control pulse power is increased to 15 W, the oscillation structure at the trailing edge will be further enhanced due to the increase in number of free carriers. In addition, when the control pulse duration and waveguide length are increased, the switching window will also quickly broaden, and split into two pulses because of the increase in the interaction length.

The initial delay time between the input control pulse and the probe signal pulse is another very important parameter, which will produce remarkable influence on the output switching window (Fig. 6), where the positive (negative) delay time means that the control (probe) pulse lags behind the probe (control) pulse. When the initial delay time is $T_d = 100$ fs, the switching window has a higher power level compared to other cases, because the group velocity of the control pulse is slower than that of the probe pulse. This is explained by the fact that by selecting the suitable initial delay time the control pulse will produce a stronger nonlinear phase shift of the probe pulse. However, when the delay time is increased to 300 fs, both pulses are hardly overlapped in time so that the influence of the control pulse on the probe pulse is very slight and the amplitude of the switching window vanishes upon a further increase in the delay time. On the other hand, when the delay time is equal to -300 fs, the switching window has a noticeable power level because the control pulse with a high energy changes the waveguide refractive index due to the generation of free carriers, which leads to the shift of the lagging phase of the probe pulse. Indeed, the obtained switching window will be virtually invariable if the negative delay time is smaller than the effective recombination time of free carriers.

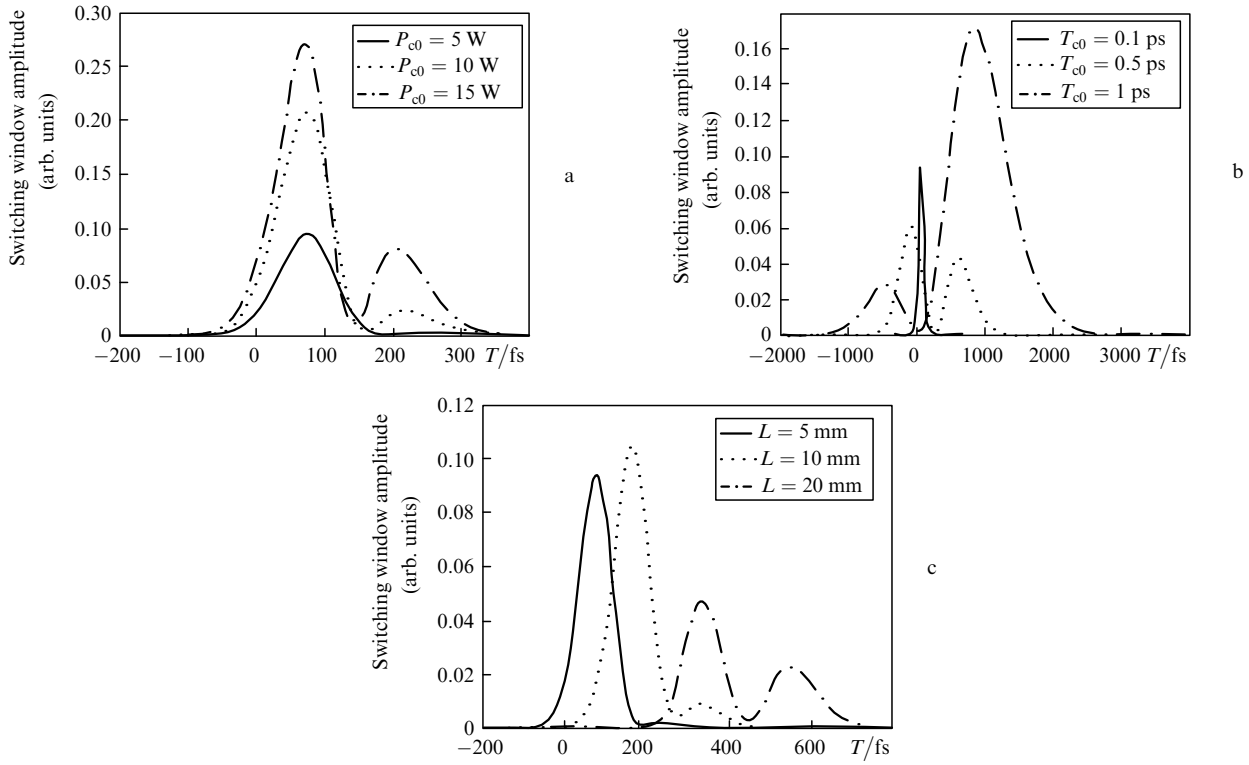

Figure 5. Amplitudes of the output switching window upon varying the input power of the control pulse at $L = 5$ mm, $T_{c0} = 100$ fs, and $P_{d0} = 100$ mW (a), duration of the control pulse at $L = 5$ mm, $P_{c0} = 5$ W and $P_{d0} = 100$ mW (b), and the waveguide length at $P_{c0} = 5$ W, $P_{d0} = 100$ mW and $T_{c0} = 100$ fs (c).

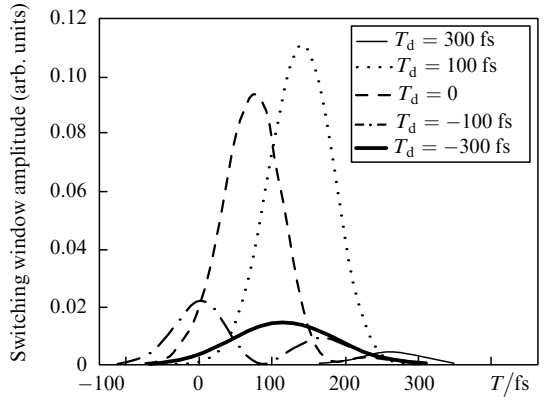

Figure 6. Amplitudes of the output switching window at different delay times and $L = 5$ mm, $P_{c0} = 5$ W and $P_{d0} = 100$ mW.

4. Conclusions

In this paper we have theoretically proposed and demonstrated the properties of the ultrafast all-optical switching window based on the symmetric MZI configuration with a SOI waveguide in both arms. To our best knowledge, we have demonstrated for the first time ultrafast all-optical switching in such waveguide devices by solving numerically the transfer equations. The high-power control pulse affects nonlinearly (through XPM, TPA, FCA, and FCD, etc.) the probe signal which provides a phase shift of the probe signal in the phase-modulating arm with respect to the phase in the reference arm and the appearance of the switching window due to the interference effect. In this paper, we have considered a cw and pulsed probe signal wave. Both cases of ultrafast optical switching are based on the identical physical principle. Because of the effect of free carriers the obtained switching window is distorted when the power and the duration of the control pulse as well as the waveguide length increase. In addition, in the case of the pulsed probe signal wave, the initial delay time also produces remarkable influence on the optical switching, which can be tuned suitably to achieve the maximum power of the switching window.

Acknowledgements. This work was supported by the Chinese National Natural Science Foundation (Grant No. 60677023) and Chinese National High Technology Research and Development Program (Grant No. 2006AA01Z240).

References

1. Soref R. *IEEE J. Sel. Top. Quantum Electron.*, **12**, 1678 (2006).
2. Jalali B., Fathpour S. *J. Lightwave Technol.*, **24**, 4600 (2006).
3. Zhou L., Poon A.W. *Opt. Lett.*, **32**, 781 (2007).
4. Dimitropoulos D., Jhaveri R., Claps R., et al. *Appl. Phys. Lett.*, **86**, 071115 (2005).
5. Leonardis F.D., Passaro V.M.N. *J. Lightwave. Technol.*, **25**, 2352 (2007).
6. Michael K., Renner H., Fathpour S., et al. *IEEE J. Quantum Electron.*, **44**, 692 (2008).
7. Dimitropoulos D., Raghunathan V., Claps R., et al. *Opt. Express*, **11**, 149 (2003).
8. Lin Q., Zhang J., Fauchet P.M., et al. *Opt. Express*, **14**, 4786 (2006).